

Implementation of higher-order absorbing boundary conditions for the Einstein equations

Oliver Rinne^{1,2,3}, Luisa T. Buchman^{3,4}, Mark A. Scheel³
and Harald P. Pfeiffer³

¹Department of Applied Mathematics and Theoretical Physics, Centre for Mathematical Sciences, Wilberforce Road, Cambridge CB3 0WA, UK

²King's College, Cambridge CB2 1ST, UK

³Theoretical Astrophysics 130-33, California Institute of Technology, Pasadena, CA 91125, USA

⁴Center for Relativity, University of Texas at Austin, Austin, TX 78712, USA

Abstract. We present an implementation of absorbing boundary conditions for the Einstein equations based on the recent work of Buchman and Sarbach. In this paper, we assume that spacetime may be linearized about Minkowski space close to the outer boundary, which is taken to be a coordinate sphere. We reformulate the boundary conditions as conditions on the gauge-invariant Regge-Wheeler-Zerilli scalars. Higher-order radial derivatives are eliminated by rewriting the boundary conditions as a system of ODEs for a set of auxiliary variables intrinsic to the boundary. From these we construct boundary data for a set of well-posed constraint-preserving boundary conditions for the Einstein equations in a first-order generalized harmonic formulation. This construction has direct applications to outer boundary conditions in simulations of isolated systems (e.g., binary black holes) as well as to the problem of Cauchy-perturbative matching. As a test problem for our numerical implementation, we consider linearized multipolar gravitational waves in TT gauge, with angular momentum numbers $\ell = 2$ (Teukolsky waves), 3 and 4. We demonstrate that the perfectly absorbing boundary condition \mathcal{B}_L of order $L = \ell$ yields no spurious reflections to linear order in perturbation theory. This is in contrast to the lower-order absorbing boundary conditions \mathcal{B}_L with $L < \ell$, which include the widely used freezing- Ψ_0 boundary condition that imposes the vanishing of the Newman-Penrose scalar Ψ_0 .

PACS numbers: 04.25.D-, 02.60.Lj, 04.25.-g

1. Introduction

Many situations of astrophysical interest can be described to good approximation as an *isolated system*: an asymptotically flat spacetime containing a compact self-gravitating source. The study of such systems requires the solution of Einstein's equations on an unbounded domain. One of the major problems in numerical relativity is how to accomplish this with finite computer resources. The most common approach is based on the Cauchy formulation of general relativity. Here the spatial computational domain is truncated at a finite distance and boundary conditions (BCs) are imposed at this artificial timelike boundary. These BCs must satisfy a number of requirements, the most important ones being that (i) the BCs must be compatible with the constraint equations that hold within the spatial slices, i.e. the BCs must be *constraint preserving*, (ii) the resulting initial-boundary value problem (IBVP) must be well posed, and

(iii) the BCs should minimize spurious reflections of gravitational radiation, i.e. the BCs should be *absorbing*. (We call BCs that completely eliminate such reflections *perfectly absorbing*.) It is important here to distinguish between spurious reflections on the one hand, and non-spurious reflections such as the backscatter off a curved background spacetime on the other hand. Perfectly absorbing BCs are defined to be exactly satisfied by the general retarded solution at the outer boundary, i.e. they only eliminate the spurious reflections but preserve non-spurious reflections such as backscatter. While considerable progress has been made on the first two requirements above, i.e. constraint preservation and well posedness, the third one on the absorbing properties of the BCs has not been addressed to the same extent. It is however of prime importance if accurate approximations to the gravitational radiation emitted by the source are to be computed, as required for instance by gravitational wave data analysis.

Theoretical progress on the construction of absorbing BCs for the Einstein field equations was made by Buchman and Sarbach in [1, 2]. A hierarchy of local BCs \mathcal{B}_L was proposed that is perfectly absorbing for all radiation with angular momentum numbers $\ell \leq L$, where L is an arbitrary given number. These BCs were obtained by studying solutions to the Bianchi equations describing linearized gravitational waves and finding a condition on the outgoing solutions that was satisfied exactly. It turns out that these BCs are a generalization to the Einstein equations of the well-known Bayliss-Turkel BCs [3] for the scalar wave equation. Initially [1], the BCs were formulated for a flat background spacetime; first-order corrections dealing with the spacetime curvature and the backscatter on a Schwarzschild black hole background were included in [2].

The objective of the present paper is to reformulate the Buchman-Sarbach BCs \mathcal{B}_L in such a way that they can be incorporated into a full set of constraint-preserving BCs for the Einstein equations, and to implement and test such BCs. Before describing our approach in more detail, we mention a number of previous works on and alternatives to absorbing BCs.

In [4], the Bayliss-Turkel BCs were implemented up to quadrupolar order ($\ell = 2$) for the scalar wave equation. The reformulation of the BCs and the numerical method used in that paper are similar to ours, but we note that we treat gravitational rather than scalar waves. A different approach to absorbing BCs is based on fast-converging series expansions of *exact nonlocal* BCs [5]. This was applied to the construction of exact absorbing BCs for the Regge-Wheeler and Zerilli (RWZ) equations in a series of papers by Lau [6, 7, 8]. The RWZ equations describe linear gravitational perturbations about a Schwarzschild black hole, and they play a central role in our approach as well. A general framework for the construction of absorbing boundaries is Cauchy-perturbative matching (CPM) [9, 10, 11, 12]. Here one matches solutions of the Einstein equations in the interior of a compact domain to solutions of the linearized equations in the exterior, represented by, for example, the RWZ equations. As we shall point out below, this approach is again closely related to ours. In addition, instead of matching to solutions of linearized gravity, one can match to an outer module solving the Einstein equations in the characteristic formulation, which is particularly well suited to the extraction of gravitational radiation (see [13] for a review article). Finally, a very promising method consists in solving the Einstein equations on hyperboloidal slices that are everywhere spacelike but that asymptotically approach null infinity (see [14] for a review article).

Our approach is based on the Buchman-Sarbach BCs, and in the following we

describe the main idea of our algorithm and the organization of this paper in more detail. We assume that close to the outer boundary, the spacetime metric can be described by linear perturbations of Minkowski spacetime in the standard coordinates. This is usually a good approximation if the outer boundary is placed sufficiently far out (we intend to generalize our work to a Schwarzschild background in the future). Note that on a flat background (unlike on a curved background where there is backscatter), the general retarded solution is purely outgoing, so in this case perfectly absorbing BCs should eliminate precisely the ingoing solution. We furthermore assume that the outer boundary is a sphere of constant coordinate radius. The original Buchman-Sarbach conditions involve higher-order radial derivatives of the Newman-Penrose scalar Ψ_0 , making it a non-trivial task to implement them numerically. Our strategy is to work with the RWZ scalars instead of Ψ_0 because on a flat-space background, the Buchman-Sarbach BCs on the RWZ scalars are precisely the same as the Bayliss-Turkel BCs for the scalar wave equation (section 2.1). Additionally, since the RWZ scalars obey closed wavelike evolution equations (the RWZ equations), we can draw on previous work in computational mathematics that successfully implements higher-order absorbing BCs for the scalar wave equation. Following [15, 16, 17], we eliminate the higher-order radial derivatives by rewriting the BCs as a system of ordinary differential equations (ODEs) for a set of auxiliary variables that need only be defined at the boundary (section 2.2). This auxiliary system is completely equivalent to the absorbing BCs imposed on the RWZ scalars.

In the interior of the computational domain, the full (nonlinear) Einstein equations are evolved. Hence we must transfer information between them and the auxiliary system at the boundary. The RWZ scalars are computed from the spacetime metric in section 2.3 following the gauge-invariant treatment of Sarbach and Tiglio [18]. In turn, we must provide boundary data for the incoming characteristic fields of the Einstein equations (section 2.4). We use a first-order formulation of these equations in generalized harmonic gauge (see [19] and references therein). In [20], a set of constraint-preserving and well-posed BCs in Sommerfeld form was proposed for the harmonic Einstein equations. These BCs contain certain free boundary data, and only very special values of these data will yield BCs that are also absorbing. The novelty of our approach lies in the construction of such absorbing boundary data from the auxiliary system at the boundary (section 2.5). We stress here that these data could equally well be obtained from exterior solutions of the RWZ equations in the CPM approach, so that our work can also be viewed as an explicit prescription for constructing BCs for the generalized harmonic Einstein equations from such perturbative solutions.

In summary, our algorithm consists in three basic steps: (i) extraction of the RWZ scalars from the spacetime metric at the boundary, (ii) evolution of the auxiliary variables at the boundary, and (iii) construction of absorbing boundary data for the Einstein equations from the auxiliary variables.

We evolve the generalized harmonic Einstein equations using a pseudospectral collocation method, the Caltech-Cornell Spectral Einstein Code (SpEC). Some details of the numerical method relevant to the present work are described in section 3.3.

As a first test problem of our implementation, we consider exact solutions of linearized gravity, multipolar gravitational waves in transverse-traceless (TT) gauge (section 3.1). The quadrupolar ($\ell = 2$) solution was first given in explicit form by Teukolsky [21], and it has recently been generalized to arbitrary ℓ in [22]. The BC $\mathcal{B}_{L=\ell}$ is perfectly absorbing for these solutions. We set initial data for $\ell = 2, 3, 4$ (section

3.2) and evolve them with this BC, $\mathcal{B}_{L=\ell}$, comparing the numerically extracted RWZ scalars with their analytical counterparts (section 3.5). We show that the difference between the two decays (at least) quadratically with amplitude so that there are no spurious reflections to linear order in perturbation theory, as expected. In contrast, $\mathcal{B}_{L<\ell}$ are shown to cause reflections at leading (linear) order. The $L = 1$ case, \mathcal{B}_1 , is equivalent to imposing the vanishing of the Newman-Penrose scalar Ψ_0 at the outer boundary, a BC that is often used in numerical relativity [23, 24, 25, 26, 27, 28, 29] and that is referred to as the freezing- Ψ_0 BC. There is a residual gauge freedom at the boundary in generalized harmonic gauge (section 3.4), and we show that our numerical results are insensitive to the particular choice of gauge boundary data. We also compute approximate reflection coefficients from our numerical evolutions and compare them with the theoretical predictions of [1] (section 3.6).

We conclude and give an outlook onto future work in section 4.

2. Formulation of the boundary conditions

In this section, we derive our reformulation of the higher-order absorbing BCs \mathcal{B}_L proposed in [1, 2]. We begin by showing how they can be expressed as BCs on the RWZ scalars (section 2.1). Radial derivatives are eliminated by introducing a system of auxiliary ODEs at the boundary (section 2.2). Next we explain how the RWZ scalars are extracted from the perturbed spacetime metric, following the gauge-invariant treatment of Sarbach and Tiglio [18] (section 2.3). Finally we describe the BCs that we impose on the Einstein equations in a first-order generalized harmonic formulation of the Einstein equations (section 2.4). Boundary data are constructed from the auxiliary system that correspond precisely to the desired absorbing BC (section 2.5).

2.1. Absorbing boundary conditions for the RWZ scalars

Although our approach is not limited to this case, we assume in this paper that spacetime near the outer boundary can be described by linear perturbations of a flat background spacetime in standard Minkowski coordinates. The spacetime metric $g_{\alpha\beta}$ is written as

$$g_{\alpha\beta} = \mathring{g}_{\alpha\beta} + \delta g_{\alpha\beta}. \quad (1)$$

We assume that the background metric $\mathring{g}_{\alpha\beta}$ is a direct product

$$\mathring{g} = \tilde{g}_{ab} dx^a dx^b + r^2 \hat{g}_{AB} dx^A dx^B, \quad (2)$$

where $\tilde{g} = -dt^2 + dr^2$ is the standard Minkowski metric on a 2-manifold \tilde{M} and $\hat{g} = d\theta^2 + \sin^2\theta d\phi^2$ is the standard metric on the 2-sphere. Throughout this paper, Greek indices α, β, \dots are spacetime indices, lower-case Latin indices a, b, \dots range over t and r , and upper-case Latin indices A, B, \dots range over θ and ϕ . The covariant derivative compatible with the metric \tilde{g} (\hat{g}) will be denoted by $\tilde{\nabla}$ ($\hat{\nabla}$) and the volume element by $\tilde{\epsilon}_{ab}$ ($\hat{\epsilon}_{AB}$). The covariant derivative $\tilde{\nabla}$ is sometimes also denoted by a vertical bar ($|$).

The hierarchy of absorbing BCs \mathcal{B}_L proposed in [1] are, for a flat-space background,

$$\mathcal{B}_L : [r^2(\partial_t + \partial_r)]^{L-1}(r^5\Psi_0) \doteq 0, \quad (3)$$

where $\hat{=}$ denotes equality at the boundary. Here the Newman-Penrose scalar Ψ_0 is evaluated for a null tetrad $(l^\alpha, k^\alpha, m^\alpha, \bar{m}^\alpha)$ adapted to the background spacetime. The BCs (3) are perfectly absorbing for all perturbations with angular momentum numbers $\ell \leq L$. We note that for $L = 1$, (3) reduces to the often-used freezing- Ψ_0 condition, $\partial_t \Psi_0 \hat{=} 0$ [23, 24, 25, 27, 26, 28, 29]. (We have not included the outer time derivative in (3); the purpose of that time derivative is to address a static background contribution to Ψ_0 , but this contribution vanishes in flat space.)

Instead of Ψ_0 , we choose to work with the RWZ scalars $\Phi_{\ell m}^{(\pm)}$ describing gauge-invariant gravitational perturbations about Schwarzschild spacetime (see [18] and references therein; of course, this includes our assumption of a flat-space background as a special case). The superscript (\pm) refers to the parity of the perturbations: $(+)$ for even and $(-)$ for odd parity. The indices ℓm refer to a spherical harmonic decomposition and will usually be suppressed in the following. We use the RWZ scalars because they have the advantage that they obey a closed evolution equation, the RWZ equation, which in flat space reads

$$\left[\partial_t^2 - \partial_r^2 + \frac{\ell(\ell+1)}{r^2} \right] \Phi^{(\pm)} = 0. \quad (4)$$

This equation arises from the scalar wave equation on $\Phi^{(\pm)}/r$ after a decomposition into spherical harmonics; it is also known as the Euler-Poisson-Darboux equation [30].

The relation between $\Phi^{(\pm)}$ and the perturbations $\delta\Psi_0$ of Ψ_0 is provided by equation 22 in [2], which for a flat-space background reduces to

$$\delta\Psi_0 = l^a l^b \tilde{\nabla}_a \tilde{\nabla}_b [r(\Phi^{(+)} + i\Phi^{(-)})] m^C m^D \hat{\nabla}_C \hat{\nabla}_D Y. \quad (5)$$

Here Y are the standard scalar spherical harmonics. We have suppressed indices ℓm on Y and $\Phi^{(\pm)}$, which are being summed over.

Equation (5) allows us to translate the BCs (3) on Ψ_0 into BCs on $\Phi^{(\pm)}$,

$$[r^2(\partial_t + \partial_r)]^{L+1} \Phi \hat{=} 0, \quad (6)$$

which holds for both parities (and hence we suppress the superscript (\pm)). We note that (6) are the well-known Bayliss-Turkel conditions [3] for the scalar wave equation on Φ/r , equation (4).

2.2. The auxiliary system at the boundary

The BCs (6), which are equivalent to the \mathcal{B}_L conditions (3), are difficult to implement numerically because they contain higher-order radial derivatives. We follow a procedure developed for the scalar wave equation in [15, 16, 17] in order to eliminate these derivatives. A set of auxiliary variables is introduced,

$$w_k \equiv r^{-(2k+1)} [r^2(\partial_t + \partial_r)]^k \Phi, \quad (7)$$

where again the parity (\pm) and the indices ℓm are suppressed. Hence these auxiliary variables obey the recursion relation

$$\left(\partial_t + \partial_r + \frac{2k+1}{r} \right) w_k = w_{k+1}. \quad (8)$$

Using the wave equation (4) and induction over k , we can prove the identity [16]

$$\left(\partial_t - \partial_r - \frac{1}{r} \right) w_k = \frac{1}{r^2} [-\ell(\ell+1) + k(k-1)] w_{k-1}. \quad (9)$$

Equations (8) and (9) can be combined to eliminate the radial derivatives,

$$\left(\partial_t + \frac{k}{r}\right) w_k = \frac{1}{2r^2}[-\ell(\ell+1) + k(k-1)]w_{k-1} + \frac{1}{2}w_{k+1}. \quad (10)$$

The BC (6) is equivalent to

$$w_{L+1} \hat{=} 0, \quad (11)$$

which closes the system of ODEs (10). We integrate (10) on the boundary for $1 \leq k \leq L$, substituting (11) and $w_0 = \Phi/r$.

2.3. Extraction of the RWZ scalars

The RWZ scalars need to be computed from the spacetime metric. We follow the gauge-invariant treatment of [18], restricted to a Minkowski background in standard coordinates. The starting point is a decomposition of the metric perturbations with respect to scalar, vector and tensor spherical harmonics. The basis harmonics are defined by

$$\begin{aligned} Y_A &\equiv \hat{\nabla}_A Y, & S_A &\equiv \hat{\epsilon}^B{}_A Y_B, \\ Y_{AB} &\equiv [\hat{\nabla}_{(A} Y_{B)}]^{\text{TF}} = \hat{\nabla}_{(A} \hat{\nabla}_{B)} Y + \frac{1}{2}\ell(\ell+1)\hat{g}_{AB}Y, & S_{AB} &\equiv \hat{\nabla}_{(A} S_{B)}, \end{aligned} \quad (12)$$

where TF denotes the tracefree part. The two parities are treated separately.

2.3.1. Odd parity. Odd-parity perturbations of the spacetime metric are decomposed as

$$\delta g_{Ab} = h_b S_A, \quad (13)$$

$$\delta g_{AB} = 2k S_{AB}. \quad (14)$$

From the amplitudes h_a and k , we construct the gauge-invariant potential

$$h_a^{(\text{inv})} = h_a - r^2 \tilde{\nabla}_a \left(\frac{k}{r^2}\right), \quad (15)$$

i.e.

$$h_t^{(\text{inv})} = h_t - \dot{k}, \quad (16)$$

$$h_r^{(\text{inv})} = h_r - r^2 \left(\frac{k}{r^2}\right)'. \quad (17)$$

Here and in the following, a dot (prime) denotes partial differentiation with respect to t (r). The Regge-Wheeler scalar $\Phi^{(-)}$ is defined as

$$\begin{aligned} \Phi^{(-)} &= -\frac{r^3}{\lambda} \tilde{\epsilon}^{ab} \tilde{\nabla}_a \left(\frac{h_b^{(\text{inv})}}{r^2}\right) = \frac{r^3}{\lambda} \left[\partial_t \left(\frac{h_r^{(\text{inv})}}{r^2}\right) - \partial_r \left(\frac{h_t^{(\text{inv})}}{r^2}\right) \right] \\ &= \frac{r}{\lambda} \left(\dot{h}_r - h_t' + \frac{2}{r} h_t \right), \end{aligned} \quad (18)$$

where $\lambda \equiv (\ell-1)(\ell+2)$. Equation (18) is valid for $\ell \geq 2$; the special case $\ell = 1$ corresponds to a non-dynamical degree of freedom (variation of the background angular momentum) that is not needed in our treatment.

2.3.2. *Even parity.* Even-parity perturbations are decomposed as

$$\delta g_{ab} = H_{ab}Y, \quad (19)$$

$$\delta g_{Ab} = Q_b Y_A, \quad (20)$$

$$\delta g_{AB} = r^2(K\hat{g}_{AB}Y + GY_{AB}). \quad (21)$$

We define the gauge parameters

$$p_a = Q_a - \frac{1}{2}r^2 G_{|a}, \quad (22)$$

i.e.

$$p_t = Q_t - \frac{1}{2}r^2 \dot{G}, \quad (23)$$

$$p_r = Q_r - \frac{1}{2}r^2 G'. \quad (24)$$

The Zerilli 1-form is given by

$$Z_a = H_{ab}r^{|b} - rK_{|a} - \frac{1}{2}\ell(\ell+1)rG_{|a} + r^{|b}\omega_{ab} + 2rv_{b|a}p^b \quad (25)$$

with $\omega_{ab} \equiv 2p_{[b|a]}$ and $v_a \equiv r^{|a}/r$, i.e.

$$Z_t = H_{tr} - r\dot{K} - \frac{1}{2}\ell(\ell+1)r\dot{G} + \dot{p}_r - p'_t, \quad (26)$$

$$Z_r = H_{rr} - rK' - \frac{1}{2}\ell(\ell+1)rG' - \frac{2}{r}p_r. \quad (27)$$

The gauge-invariant potential is

$$K^{(\text{inv})} = K + \frac{1}{2}\ell(\ell+1)G - \frac{2}{r}r^{|b}p_b = K + \frac{1}{2}\ell(\ell+1)G - \frac{2}{r}p_r. \quad (28)$$

Finally, we obtain the Zerilli scalar

$$\Phi^{(+)} = -\frac{r}{\lambda\ell(\ell+1)}(2r^{|a}Z_a + \lambda K^{(\text{inv})}) = -\frac{r}{\lambda\ell(\ell+1)}(2Z_r + \lambda K^{(\text{inv})}). \quad (29)$$

Again, this formula is valid for $\ell \geq 2$; the non-dynamical cases $\ell = 0$ (variation of the background mass) and $\ell = 1$ (pure gauge) are not needed.

2.4. Boundary conditions for the generalized harmonic Einstein equations

Next we describe the BCs that we impose on the actual Einstein equations that are being solved in the interior of the domain. We consider a first-order formulation of these equations in generalized harmonic coordinates (see [19] and references therein). Generalized harmonic spacetime coordinates x^α are defined by

$$\square x^\alpha = -g^{\beta\gamma}\Gamma^\alpha_{\beta\gamma} = H^\alpha, \quad (30)$$

where \square is the scalar d'Alembert operator of the spacetime metric $g_{\alpha\beta}$, $\Gamma^\alpha_{\beta\gamma}$ are its Christoffel symbols, and H^α are freely specifiable gauge source functions. The evolved variables are $g_{\alpha\beta}$ and their first derivatives

$$\Pi_{\alpha\beta} = -t^\gamma\partial_\gamma g_{\alpha\beta}, \quad (31)$$

$$\Phi_{i\alpha\beta} = \partial_i g_{\alpha\beta}, \quad (32)$$

where t^α is the future-directed unit timelike normal to the $t = \text{const}$ slices. Greek indices α, β, \dots are spacetime indices and Latin indices i, j, \dots from the middle of the alphabet are spatial. Boundary data must be specified for the incoming fields at the boundary,

$$u_{\alpha\beta}^{1-} = \Pi_{\alpha\beta} - n^i\Phi_{i\alpha\beta} - \gamma_2 g_{\alpha\beta}, \quad (33)$$

where n^α is the outward-pointing unit spatial normal to the boundary on the $t = \text{const}$ slices, $t^\alpha n_\alpha = 0$. The parameter γ_2 appears due to the addition of constraint-damping terms to the evolution equations; let us also define

$$\tilde{u}_{\alpha\beta}^{1-} \equiv u_{\alpha\beta}^{1-} + \gamma_2 g_{\alpha\beta} = \Pi_{\alpha\beta} - n^i \Phi_{i\alpha\beta}. \quad (34)$$

Our BCs are of a similar type as those considered in [20] but with boundary data derived from our auxiliary system at the boundary as described in the following.

The incoming fields are split into three different pieces by three projection operators P^C , P^P and P^G (referring to constraint, physical and gauge BCs). In order to define them, we introduce the null vectors $l^\alpha \equiv (t^\alpha + n^\alpha)/\sqrt{2}$ and $k^\alpha \equiv (t^\alpha - n^\alpha)/\sqrt{2}$ and the spatial metric induced on the boundary, $P_{\alpha\beta} \equiv g_{\alpha\beta} + t_\alpha t_\beta - n_\alpha n_\beta$. The projection operators are given by

$$P_\alpha^{C\gamma\delta} = 2k^{(\gamma} \delta_\alpha^{\delta)} - k_\alpha g^{\gamma\delta}, \quad (35)$$

$$P_{\alpha\beta}^{P\ \gamma\delta} = P_\alpha^\gamma P_\beta^\delta - \frac{1}{2} P_{\alpha\beta} P^{\gamma\delta}, \quad (36)$$

$$P_\alpha^{G\gamma\delta} = \delta_\alpha^\gamma l^\delta. \quad (37)$$

The complements of the kernels of these three projection operators are disjoint and together they span the space of all symmetric 2-tensors.

We impose constraint-preserving BCs by requiring the generalized harmonic gauge constraint (30) to hold at the boundary. This can be written in the form

$$P_\alpha^{C\gamma\delta} \tilde{u}_{\gamma\delta}^{1-} \hat{=} F_\alpha^C, \quad (38)$$

where F_α^C is a function of outgoing and zero-speed characteristic fields and gauge source functions, see equation 32 of [27]. The rank-2 projection operator P^P describes the BCs on the two gravitational degrees of freedom. They take the form

$$P_{\alpha\beta}^{P\ \gamma\delta} \tilde{u}_{\gamma\delta}^{1-} \hat{=} F_{\alpha\beta}^P. \quad (39)$$

Here $F_{\alpha\beta}^P$ are boundary data that will be constructed in the following subsection from our auxiliary variables at the boundary; thus these ‘‘physical’’ boundary data implement the absorbing BC \mathcal{B}_L that we want to impose. The remaining BCs

$$P_\alpha^{G\gamma\delta} \tilde{u}_{\gamma\delta}^{1-} \hat{=} F_\alpha^G \quad (40)$$

are related to the residual gauge freedom within the generalized harmonic gauge: we can still perform infinitesimal coordinate transformations of the coordinates $x^\alpha \rightarrow x^\alpha + \xi^\alpha$ provided that ξ^α obeys the wave equation. The F_α^G are free data that will be specified so that our BCs are compatible with the exact solution that we want to reproduce. In realistic simulations without an exact solution at hand, we would take the F_α^G to vanish.

The BCs (38)–(40) were proven in [20, 31] to yield a well-posed IBVP for the Einstein equations in harmonic gauge. This result cannot be directly applied to our formulation because (i) whereas the second-order Einstein equations are considered in [20, 31], our evolution system [19] is a first-order reduction thereof, and (ii) rather than being *a priori* given functions of time, the boundary data $F_{\alpha\beta}^P$ in (39) depend implicitly on the dynamical fields, as we shall see in the following subsection. Nevertheless, it has been shown in [32] that the absorbing BCs \mathcal{B}_L are well posed for the second-order Einstein equations in harmonic gauge at least in the high-frequency limit. Therefore, it seems likely that our method leads to a well-posed IBVP; a proof is beyond the scope of this paper.

2.5. Construction of absorbing boundary data

Finally, we show how to construct boundary data $F_{\alpha\beta}^{\text{P}}$ in (39) that correspond to \mathcal{B}_L . Recall that we are assuming that the fields can be linearized about flat space close to the outer boundary, which is taken to be a sphere $r = \text{const}$. Hence we have $t^\alpha = \delta_t^\alpha$ and $n^\alpha = \delta_r^\alpha$ for the background, and the incoming fields (without the γ_2 term) in (34) read

$$\tilde{u}_{\alpha\beta}^{1-} = -(\partial_t + \partial_r)g_{\alpha\beta}. \quad (41)$$

The only non-vanishing components of the ‘‘physical’’ BCs (39) are the angular components, $\alpha\beta = AB$. We find

$$F_{AB}^{\text{P}} \hat{=} P_{AB}^{\text{P}} \gamma^\delta \tilde{u}_{\gamma\delta}^{1-} = -r^2(\partial_t + \partial_r)(r^{-2}\delta g_{AB}^{\text{TF}}), \quad (42)$$

where TF denotes the trace-free part with respect to the metric \hat{g} on the 2-sphere. We now derive expressions for the right-hand side of the above equation in the RWZ formalism that involve the auxiliary variables at the boundary.

2.5.1. Odd parity. From (16) and (17) we obtain

$$h_t^{(\text{inv})} + h_r^{(\text{inv})} = h_t + h_r - r^2(\partial_t + \partial_r)(r^{-2}k). \quad (43)$$

On the other hand [18], the gauge-invariant potential is related to the Regge-Wheeler scalar via $h^{(\text{inv})} = \tilde{*}d(r\Phi^{(-)})$, where $\tilde{*}$ denotes the Hodge dual with respect to \hat{g} . Thus,

$$h_t^{(\text{inv})} + h_r^{(\text{inv})} = -(\partial_t + \partial_r)(r\Phi^{(-)}) = -r^2w_1^{(-)} - rw_0^{(-)}, \quad (44)$$

where we have substituted the definition (7) of the auxiliary variables. Combining (43) and (44),

$$r^2(\partial_t + \partial_r)(r^{-2}k) = h_t + h_r + r^2w_1^{(-)} + rw_0^{(-)}. \quad (45)$$

Finally (45) is substituted in the expression (42) for the boundary data (noting (14)),

$$\begin{aligned} F_{AB}^{\text{P}} &= -r^2(\partial_t + \partial_r)(r^{-2}\delta g_{AB}^{\text{TF}}) = -2r^2 [(\partial_t + \partial_r)(r^{-2}k)] S_{AB} \\ &= -2 [h_t + h_r + r^2w_1^{(-)} + rw_0^{(-)}] S_{AB}. \end{aligned} \quad (46)$$

Here we see clearly how the information from the auxiliary system that implements \mathcal{B}_L enters the boundary data for the Einstein equations. We note that $S_{AB} = 0$ for $\ell \leq 1$, which justifies our neglecting this special case.

2.5.2. Even parity. From (26) and (27) we obtain

$$Z_t + Z_r = -\frac{\lambda}{2}r(\partial_r + \partial_t)G - r(\partial_t + \partial_r)K + \dot{Q}_r - Q'_t - \frac{2}{r}Q_r + H_{tr} + H_{rr}. \quad (47)$$

Using the definitions [18] $d\zeta = Z$ and $\Phi^{(+)} = \zeta/\lambda$, we find the alternate expression

$$Z_t + Z_r = \lambda(\partial_t + \partial_r)\Phi^{(+)} = \lambda rw_1^{(+)}, \quad (48)$$

where we have substituted the definition (7) of the auxiliary variables. Combining (47) and (48),

$$r^2(\partial_t + \partial_r)G = -2r^2w_1^{(+)} - \frac{2}{\lambda}r^2(\partial_t + \partial_r)K + \frac{2r}{\lambda}(\dot{Q}_r - Q'_t - \frac{2}{r}Q_r + H_{tr} + H_{rr}). \quad (49)$$

Finally (49) is substituted in the expression (42) for the boundary data (noting (21)),

$$\begin{aligned} F_{AB}^{\text{P}} &= -r^2(\partial_t + \partial_r)(r^{-2}\delta g_{AB}^{\text{TF}}) = -[r^2(\partial_t + \partial_r)G] Y_{AB} \\ &= -\left[-2r^2w_1^{(+)} - \frac{2}{\lambda}r^2(\partial_t + \partial_r)K + \frac{2r}{\lambda}(\dot{Q}_r - Q'_t - \frac{2}{r}Q_r + H_{tr} + H_{rr})\right] Y_{AB}. \end{aligned} \quad (50)$$

We note that $Y_{AB} = 0$ for $\ell \leq 1$, which justifies our neglecting this special case.

2.5.3. Application to Cauchy-perturbative matching. We remark that the auxiliary variables $w_k^{(\pm)}$ ($k = 0, 1$) appearing on the right-hand sides of (46) and (50) could equally well be computed from a given exterior solution $\Phi^{(\pm)}$ of the RWZ equations, using the definition (7) of the auxiliary variables. Hence we have shown how to construct BCs for the generalized harmonic Einstein equations in the CPM approach.

3. Numerical tests

In this section, we present numerical tests of our formulation of higher-order absorbing BCs \mathcal{B}_L derived in section 2.

We evolve initial data representing exact wavelike solutions of the *linearized* Einstein equations using a *fully nonlinear* evolution code that implements \mathcal{B}_L . We extract the RWZ scalars at the boundary and compare them to the corresponding exact linearized solutions in order to assess the amount of spurious reflections from the boundary. Because we evolve the full nonlinear equations but our initial data and the solutions with which we compare are based on linearized theory, our comparisons will disagree because of nonlinear effects; we repeat each run at several different amplitudes in order to separate these nonlinear effects from the boundary reflections we are studying.

In section 3.1, we describe exact solutions of linearized gravity representing multipolar (with angular momentum number ℓ) gravitational waves in TT gauge. We compute the RWZ scalars and demonstrate that $\mathcal{B}_{L=\ell}$ is perfectly absorbing for these solutions. In section 3.2, we describe our use of these solutions to set up initial data for numerical evolution. After briefly explaining our pseudo-spectral numerical method (section 3.3) and our treatment of gauge BCs (section 3.4), we discuss our numerical results in section 3.5. Finally, in section 3.6, we estimate reflection coefficients from our numerical evolutions with the various BCs and compare them with the predictions of [1].

3.1. Multipolar gravitational wave solutions

Teukolsky [21] gave the explicit form of the metric for a quadrupolar ($\ell = 2$) gravitational wave linearized about flat space in the TT gauge. This solution has recently been generalized to arbitrary angular momentum number ℓ in [22]. The solutions are characterized by freely specifiable mode functions $F_{\text{out}}(r-t)$, $F_{\text{in}}(r+t)$ for even parity and $G_{\text{out}}(r-t)$, $G_{\text{in}}(r+t)$ for odd parity. They describe outgoing and incoming waves, respectively. There is an independent solution for each m , $-\ell \leq m \leq \ell$.

We note that whereas the solution for the metric is real, the spherical harmonics are complex for $m \neq 0$. As a consequence, the amplitudes appearing in the spherical harmonic decomposition, equations (13)–(14) and (19)–(21), as well as the RWZ scalars $\Phi_{\ell m}^{(\pm)}$ obey the reality conditions

$$u_{\ell m}^* = (-1)^m u_{\ell, -m}, \quad (51)$$

where \star denotes complex conjugation. More precisely, let us consider the solution for a single mode $(\ell, m) = (\hat{\ell}, \hat{m})$. Then we may write for any of the aforementioned quantities

$$u_{\ell m} = c_{\ell m} u(t, r), \quad (52)$$

where $u(t, r)$ is a real function and the $c_{\ell m}$ are complex coefficients given by

$$\text{if } \hat{m} \geq 0 : \quad c_{\ell, \hat{m}} = c_{\ell, -\hat{m}} = \frac{1}{2}, \quad c_{\ell m} = 0 \text{ otherwise,} \quad (53)$$

$$\text{if } \hat{m} < 0 : \quad c_{\ell, \hat{m}} = \frac{1}{2}, \quad c_{\ell, -\hat{m}} = -\frac{1}{2}, \quad c_{\ell m} = 0 \text{ otherwise.} \quad (54)$$

In the following, we only display the real functions $u(t, r)$. The $\ell = 2$ solutions in [21, 22] differ by an overall constant factor; we use the normalization of [22] throughout.

From the explicit form of the metric, equations 4 and 5 in [22], we read off the amplitudes

$$\begin{aligned} H_{tt} = H_{tr} = 0, \quad H_{rr} = A, \quad Q_t = 0, \\ Q_r = rB, \quad K = -\frac{1}{2}A, \quad G = C \end{aligned} \quad (55)$$

for even parity and

$$h_t = 0, \quad h_r = rK, \quad k = \frac{1}{2}r^2L \quad (56)$$

for odd parity, where the quantities A, B, C and K, L on the right-hand sides are the radial functions defined in equations 8 and 9 in [22].

Next we compute the RWZ scalars as described in section 2.3. For brevity, we focus on $\ell = 2$. In terms of the mode functions, the outgoing solution is found to be

$$\Phi^{(+)} = F_{\text{out}}^{(4)} - \frac{3F_{\text{out}}^{(3)}}{r} + \frac{3F_{\text{out}}^{(2)}}{r^2}, \quad (57)$$

$$\Phi^{(-)} = G_{\text{out}}^{(3)} - \frac{3G_{\text{out}}^{(2)}}{r} + \frac{3G_{\text{out}}^{(1)}}{r^2}, \quad (58)$$

where $F^{(k)}(x) \equiv d^k F(x)/dx^k$. It can be verified easily that the RWZ scalars given in (57) and (58) obey the RWZ equation (4).

The auxiliary variables (7) for the outgoing solution are found to be

$$w_1^{(+)} = \frac{3F_{\text{out}}^{(3)}}{r^3} - \frac{6F_{\text{out}}^{(2)}}{r^4}, \quad w_2^{(+)} = \frac{6F_{\text{out}}^{(2)}}{r^5}, \quad w_3^{(+)} = 0, \quad (59)$$

and similarly for odd parity. We see that the BC \mathcal{B}_2 corresponding to $w_3^{(+)} \hat{=} 0$ (equation (11)) is perfectly absorbing for this solution (it is satisfied identically by the outgoing solution), whereas the freezing- Ψ_0 condition \mathcal{B}_1 corresponding to $w_2^{(+)} \hat{=} 0$ is not, although the correction in $w_2^{(+)}$ falls off quite fast with boundary radius ($\sim r^{-5}$). More generally for arbitrary ℓ , $\mathcal{B}_{L=\ell}$ is perfectly absorbing whereas $\mathcal{B}_{L<\ell}$ is not.

3.2. Initial data for numerical evolutions

The initial data for our numerical evolutions are taken from the exact linearized multipolar wave solutions described in section 3.1, evaluated at $t = 0$. We shall consider the cases $\ell = 2, 3, 4$. For definiteness, we choose $m = 2$ throughout; we have checked that our results are insensitive to the particular choice of m .

We take an outgoing wave with mode function

$$F_{\text{out}}(x) = A \exp \left[-\frac{(x - r_0)^2}{\sigma^2} \right]. \quad (60)$$

The parameters are taken to be $r_0 = 15$ and $\sigma = 1.5$. These choices are dictated by the requirement that at the outer boundary radius R of our computational domain, which we place at $R = 30$, the wave initially vanish to numerical roundoff error; this guarantees that the initial data are consistent with the boundary data at $R = 30$.

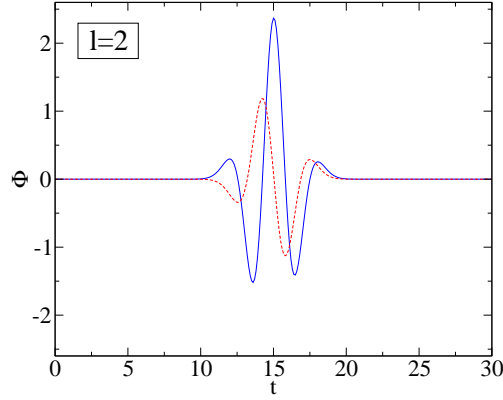


Figure 1. Outgoing linearized gravitational wave with multipolar indices $\ell = m = 2$ and mode function (60) with parameters $A = 1$, $r_0 = 15$ and $\sigma = 1.5$. Shown are the exact solutions (57) for the Zerilli scalar $\Phi^{(+)}$ (solid) and (58) for the Regge-Wheeler scalar $\Phi^{(-)}$ (dashed) as functions of time, evaluated at $R = 30$.

Figure 1 shows the exact solutions for the RWZ scalars (for $\ell = 2$) as functions of time evaluated at the outer boundary $r = R = 30$.

Although we will evolve the full nonlinear Einstein equations, we do not solve the full nonlinear constraints initially (of course the exact solution satisfies the constraints to linear order). This is because we are interested only in comparing the numerical solution with the exact solution to linear order in perturbation theory.

3.3. Numerical evolution method

Our numerical implementation uses the Caltech-Cornell Spectral Einstein Code (SpEC), which is based on a pseudo-spectral collocation method described in more detail for example in [24]. We evolve the first-order generalized harmonic form of the Einstein equations as described in [19]. The gauge-source functions H^α in (30) are taken to be zero when that equation is evaluated in Cartesian components, compatible with the TT gauge of the exact linearized solution.

The computational domain for the evolutions presented here is a sphere of radius $R = 30$. It is subdivided into a small central sphere of radius $\Delta r = 7.5$ surrounded by three spherical shells, each of extent Δr . In the spherical shells, each Cartesian tensor component of each tensor field is expanded in Chebyshev polynomials in the radial direction and in spherical harmonics $Y_{\ell m}(\theta, \phi)$ in the angular directions. In the central sphere, the numerical solution is expanded in the basis functions introduced by Matsushima and Marcus [33] with parameters $\alpha = 1$ and $\beta = 2$: each Cartesian tensor component is expanded as $f(r, \theta, \phi) = \sum_{n\ell m} f_{n\ell m} Q_{n\ell}(r) Y_{\ell m}(\theta, \phi)$, where $Q_{n\ell}(r)$ depends on the index ℓ and $Q_{n\ell}(r) \sim r^\ell$ near the origin. The number of radial expansion coefficients is the same in each subdomain, and is denoted by N_r . Likewise, the highest retained spherical harmonic index is the same in each subdomain, and is denoted by N_ℓ . In all subdomains we retain all spherical harmonic m coefficients with $|m| \leq \ell$.

For the RWZ formalism, we need to compute the expansion coefficients of various tensors with respect to the basis $Y, Y_A, S_A, Y_{AB}, S_{AB}$ defined in (12). The SpEC code

is already capable of computing expansions in *spin-weighted* spherical harmonics. The conversion between the two bases is detailed in Appendix A. We note that there is no need to use spin-weighted harmonics, it is simply convenient in the SpEC code.

The evolution equations are integrated in time using a fourth-order Runge-Kutta scheme, with a Courant factor $\Delta t/\Delta x_{\min}$ of at most 2.25, where Δx_{\min} is the smallest distance between two neighbouring collocation points. (This method of defining a Courant factor for a pseudospectral code with uneven grid spacing is only a crude approximation; so in practice, numerical stability can be achieved with Courant factors larger than unity.) As described in [24], the top four coefficients in the *tensor* spherical harmonic expansion of each of our evolved quantities are set to zero after each time step; this eliminates an instability associated with the inconsistent mixing of tensor spherical harmonics in our approach. The auxiliary ODEs (10) are integrated using the same Runge-Kutta scheme.

The BCs on the incoming fields of the generalized harmonic Einstein equations at the outer boundary and at the internal boundaries between neighbouring subdomains are enforced using a penalty method [34]. At the internal boundaries, the incoming fields on each boundary are set (weakly via the penalty method) equal to the corresponding outgoing field on the neighbouring boundary. At the outer boundary, we always impose the constraint-preserving boundary conditions (38) on the constrained degrees of freedom, and we vary the BCs on the physical and gauge degrees of freedom as described below.

3.4. Boundary conditions on gauge fields

Besides the BCs on the physical degrees of freedom that are the subject of this paper, and those on the constraint degrees of freedom for which we choose equation (38), we must also specify a BC (40) on the gauge degrees of freedom. The multipolar gravitational waves described in section 3.1 are in TT gauge,

$$\delta g_{tt} = 0, \quad \delta g_i{}^i = 0, \quad \overset{\circ}{\nabla}_j \delta g^{ij} = 0, \quad (61)$$

where $\overset{\circ}{\nabla}$ is the flat-space covariant derivative. This implies that the harmonic gauge condition (30) with vanishing gauge source functions H^α —when evaluated in Cartesian components—is satisfied in linearized theory. However, the gauge boundary data F_α^G in (40) do not vanish for this solution; we have to specify them explicitly. One might be tempted to replace the gauge BC (40) with

$$t^\alpha u_{\alpha\beta}^{1-} = 0, \quad (62)$$

which is compatible with TT gauge. Unfortunately, the ensuing IBVP is ill posed [35]. Alternatively, one might hope to transform the solution to a different gauge such that both the harmonic gauge condition and the homogeneous version of the gauge BC (40) are satisfied; however, it turns out that this cannot be achieved for a purely outgoing solution [36].

Hence we have decided to specify gauge boundary data F_α^G that are computed from the exact linearized solution. Alternatively, we set $F_\alpha^G = 0$. The latter is compatible with the exact solution at early times provided the initial data have compact support and the outer boundary is sufficiently far out. Once the outgoing wave hits the outer boundary, there will be a (small) reflection which is pure gauge and hence should not affect the physical gravitational radiation as represented by the RWZ scalars.

3.5. Numerical results

Here we describe the results of evolving initial data describing exact solutions of the *linearized* Einstein equations (section (3.1)) using our *fully nonlinear* evolution code that includes our new absorbing BCs. Because we will compare the RWZ scalars extracted from our nonlinear numerical evolution with their exact (linearized) values, our comparisons will disagree because of nonlinear effects. Therefore we repeat each run at several different amplitudes in order to separate these nonlinear effects from the boundary reflections of interest. The numerical resolution (N_r, N_ℓ) is chosen high enough such that the numerical truncation error is negligible compared to the differences we are studying.

We begin with the quadrupolar solution ($\ell = 2$). Here we consider amplitudes in the range $10^{-3.49} \leq A \leq 10^{-1.39}$. We performed a convergence test which showed that for any amplitude in this range, a numerical resolution of $N_r = 81$, $N_\ell = 8$ is sufficient to remove the effects of numerical truncation error.

First we consider \mathcal{B}_2 , which was shown in section 3.1 to be perfectly absorbing for the $\ell = 2$ solution. As mentioned in section 3.4, there is some freedom in the choice of gauge boundary data F_α^G . First we compute these functions F_α^G from the exact solution; with this choice of boundary gauge, the entire spacetime metric should agree with the exact linearized solution. We compute from the numerical evolution the $\ell = m = 2$ component of the RWZ scalars, evaluated at the outer boundary, for both an odd-parity and an even-parity wave (this is the only nonvanishing component in the exact solution, up to the reality condition (51)). We then compute the same quantity from the exact linearized solution, and plot the difference in figure 2. This difference has been normalized by the amplitude A , so that if the quantity plotted decreases at least linearly with decreasing amplitude, the difference between the numerical and exact solution decreases at least quadratically with amplitude, i.e. the two solutions agree to linear order in perturbation theory. This is indeed what we see in figure 2 (the decay exponent of the normalized difference is found to be close to 2). Similar behaviour is found for the remaining components of the RWZ scalars, which vanish for the exact solution.

Next we replace the analytic gauge BC with the homogeneous one, $F_\alpha^G = 0$, also referred to as a *freezing* gauge BC. The results are virtually unchanged (figure 3). This demonstrates that the ambiguity in the choice of gauge BC has no effect on the gauge-invariant quantities. In all further evolutions discussed below, we will continue to use the freezing gauge BC.

As discussed in section 3.1, we expect the freezing gauge BC to cause a small gauge wave reflection. This should show up in gauge-dependent quantities such as the spacetime metric. Figure 4 shows the component g_{tx} of the metric, which vanishes for the exact solution because of the TT gauge. Indeed this quantity is found to decay quadratically with amplitude when analytical gauge BCs are used (left panel of figure 4; note again the quantity plotted has been normalized by the amplitude). For the freezing gauge BC (right panel), the curves begin to overlap for sufficiently small amplitudes. This indicates that the numerical solution differs from the exact solution to leading (linear) order in perturbation theory. We had to use somewhat smaller amplitudes for this plot ($10^{-5.49} \leq A \leq 10^{-3.49}$) so that the nonlinear effects are smaller than the gauge wave reflection that we are looking for.

We now repeat the evolution shown in figure 3, but using \mathcal{B}_1 ; this corresponds to freezing Ψ_0 at the boundary. As shown analytically in section 3.5, \mathcal{B}_1 is *not* compatible

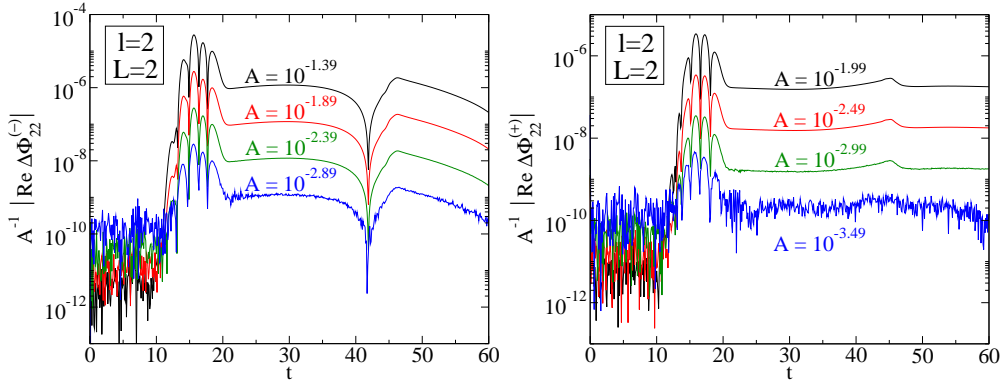


Figure 2. Difference between the numerically-extracted RWZ scalar Φ_{22} and its exact linearized value, evaluated on the outer boundary, and divided by the amplitude A . The exact linearized solution and the initial data for the evolution contain only the $\ell = 2, m = 2$ mode of odd (left panel) or even (right panel) parity. The evolution uses \mathcal{B}_2 and analytic gauge BCs. Roundoff effects become visible at the smallest amplitude.

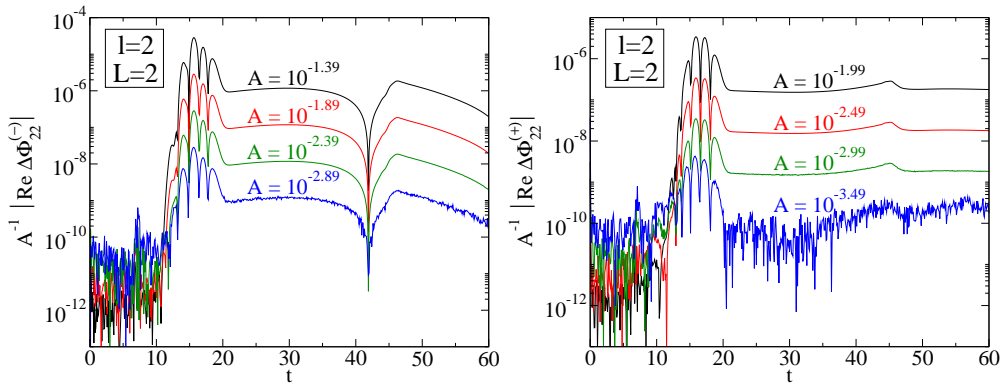


Figure 3. Same as figure 2, except freezing gauge BCs are used in the evolution.

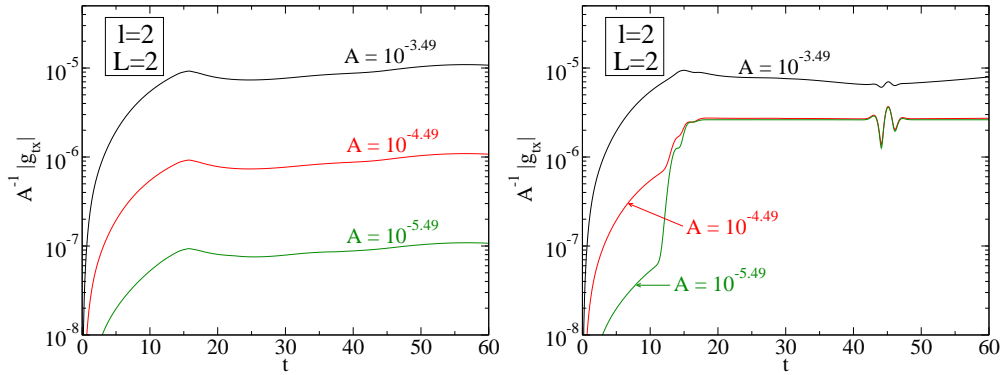


Figure 4. The component g_{tx} of the metric, normalized by the amplitude A , for the even-parity evolutions shown in figures 2 and 3. The two panels are identical except for the gauge BCs used: analytic (left panel) and freezing (right panel).

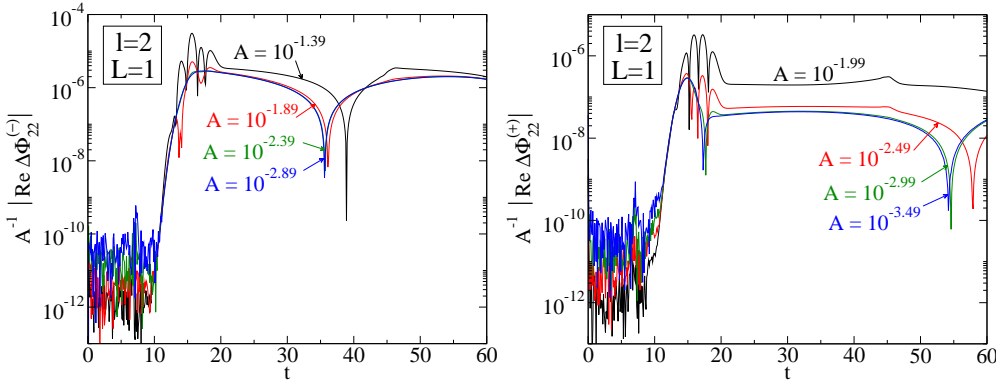


Figure 5. Same as figure 3, except the evolution uses BC \mathcal{B}_1 .

with the exact outgoing solution. Figure 5 shows the RWZ scalars for this numerical evolution. The curves corresponding to smaller amplitudes nearly overlap, which implies that the numerical solution differs from the exact one at linear order. Note however that the normalized difference is still relatively small (about 10^{-6} or 10^{-7} , depending on the parity). The remaining modes of the RWZ scalars not shown here behave in the same way as for \mathcal{B}_2 , i.e. they decay at least quadratically with amplitude (note these modes vanish for the exact linearized solution).

We now turn to evolutions of octupolar ($\ell = 3$) waves. Here we consider amplitudes in the range $10^{-3.5} \leq A \leq 10^{-2}$, and we find that a numerical resolution of $N_r = 91$, $N_\ell = 10$ is sufficient to remove the effects of numerical truncation error for the amplitudes in this range. Figure 6 shows evolutions using \mathcal{B}_1 , \mathcal{B}_2 , and \mathcal{B}_3 . (We continue to use freezing gauge BCs.) As expected from the analytic discussion in section 3.1, \mathcal{B}_3 is found to be consistent with the exact linearized solution, whereas \mathcal{B}_1 and \mathcal{B}_2 are not. To show the dependence on the order of the BC more clearly, in figure 7 we plot the time integrals of the curves in figure 6 versus the amplitude. We see clearly how for \mathcal{B}_1 and \mathcal{B}_2 , this time integral saturates in the limit of small amplitudes, at a level which is lower for \mathcal{B}_2 than for \mathcal{B}_1 . This saturation to a horizontal line at small amplitudes again indicates a difference between the numerical and exact solution that decays only linearly with amplitude. The reason why these curves increase for larger amplitudes is because nonlinear effects become important. The curve for \mathcal{B}_3 behaves differently: it continues to decay with decreasing amplitude. (The slight levelling off of this curve at the smallest amplitude is caused by numerical round-off effects.) This is consistent with the theoretical prediction that \mathcal{B}_3 is perfectly absorbing for waves with $\ell \leq 3$, so the difference between the numerical and exact linear solution is (almost) entirely due to nonlinear terms. Again, we find a nearly quadratic decay of the \mathcal{B}_3 curve in figure 7, corresponding to a nearly cubic decay of the difference between the numerical and exact solution.

Finally we evolve the $\ell = 4$ solution. Here we consider amplitudes in the range $10^{-4} \leq A \leq 10^{-2.5}$ and the numerical resolution is $N_r = 101$, $N_\ell = 12$. Figure 8 compares \mathcal{B}_1 (corresponding to freezing Ψ_0 at the boundary) and \mathcal{B}_4 (which is predicted to be perfectly absorbing for this solution). Again the numerical results confirm that \mathcal{B}_4 is compatible with the exact linearized solution whereas \mathcal{B}_1 is not.

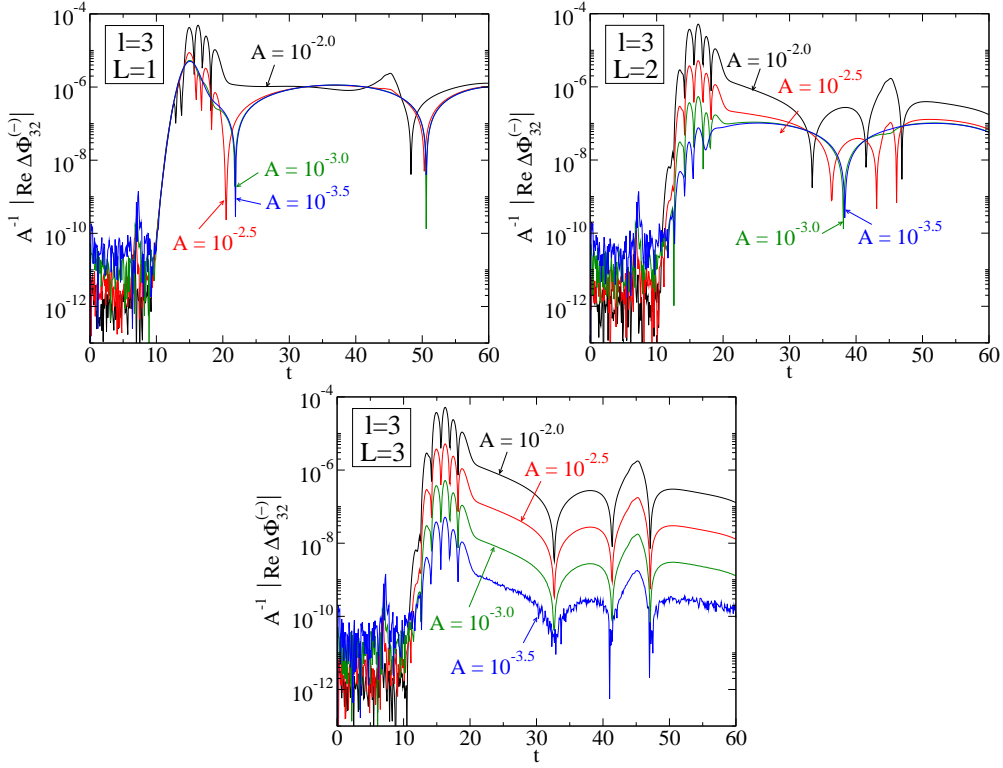


Figure 6. Difference between the numerically-extracted RWZ scalar $\Phi_{32}^{(-)}$ and its exact linearized value, evaluated on the outer boundary, and divided by the amplitude A . The exact linearized solution and the initial data for the evolution contain only the $\ell = 3, m = 2$ odd-parity mode. The different panels correspond to absorbing BCs \mathcal{B}_L with $L = 1, 2$, and 3. Freezing gauge BCs are used.

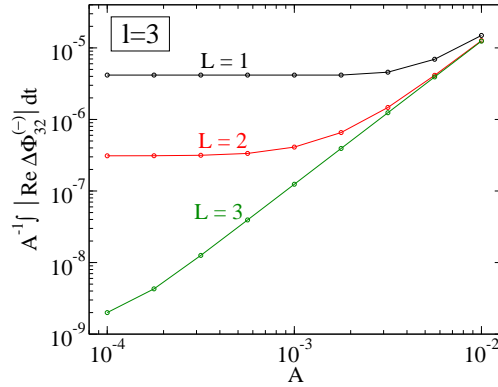


Figure 7. Time integral of the curves shown in figure 6, plotted against the amplitude A . The different curves correspond to absorbing BCs \mathcal{B}_L with $L = 1, 2$ and 3.

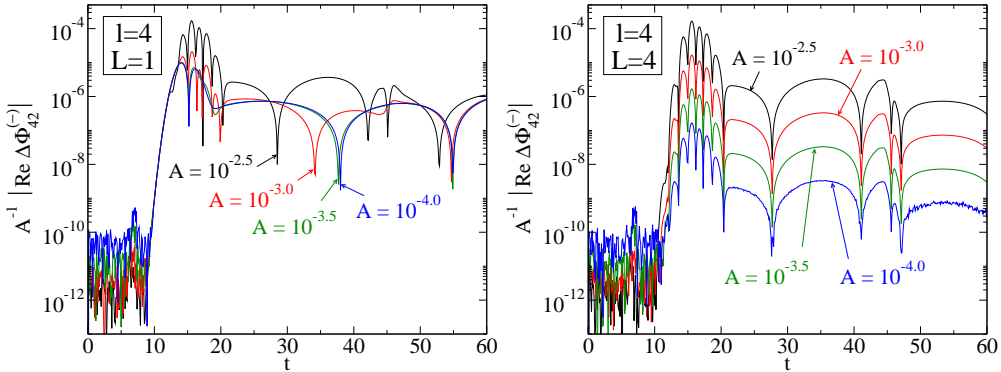


Figure 8. Same as figure 6, except the exact linearized solution and the initial data for the evolution now contain only the odd-parity $\ell = 4, m = 2$ mode. The different panels correspond to \mathcal{B}_L with $L = 1$ and 4.

3.6. Comparison with the predicted reflection coefficients

In [1], solutions to the linearized Bianchi equations with higher-order absorbing BCs equivalent to \mathcal{B}_L were studied theoretically. For monochromatic radiation, analytical expressions for the reflection coefficients relating the amplitude of an outgoing wave to the spurious reflected ingoing wave were derived (equation 96 of [1]). In this section, we compare these predicted reflection coefficients with the numerical results presented in section 3.5.

The predicted reflection coefficients in [1] are given as functions of $2\pi R/\lambda$, where λ is the wavelength of the radiation and R is the radius of a spherical outer boundary. Our numerical tests, however, evolve wave packets and not monochromatic waves. So to obtain the reflection coefficients as a function of λ for our numerical evolutions, we proceed as follows. We measure the radiation reflected off the outer boundary by taking the difference between our numerically-evolved solution and the exact linearized solution at the boundary, which we have plotted as a function of time in figures 5, 6 and 8. In order to minimize the nonlinear effects, the lowest amplitudes are used ($A = 10^{-2.89}$ for $\ell = 2$, $A = 10^{-3.5}$ for $\ell = 3$ and $A = 10^{-4}$ for $\ell = 4$). Taking the Fourier transform of any of the curves in these figures (prior to taking absolute values) yields the difference as a function of frequency, from which we can obtain the difference as a function of wavelength, $\Delta\Phi(\lambda)$. Similarly, we can obtain $\Phi(\lambda)$ by taking the Fourier transform of the exact linearized solution $\Phi(t)$, evaluated at the boundary. Given these quantities, we define the reflection coefficient at any particular wavelength λ as $\Delta\Phi(\lambda)/\Phi(\lambda)$.

The values of both the analytical and numerical reflection coefficients are plotted as a function of λ/R in figure 9, for radiation with angular momentum numbers $\ell = 2, 3, 4$ and absorbing BCs $\mathcal{B}_{L < \ell}$. This demonstrates the importance of higher-order BCs when the numerical simulation contains multipolar radiation. For example, assume the outer boundary is located at twice the characteristic wavelength of the simulation, so that $\lambda/R = 0.5$. Then, for radiation with $\ell = 3$ and freezing- Ψ_0 BCs (\mathcal{B}_1), the predicted errors due to spurious reflections off the boundary are 3×10^{-4} . The use of \mathcal{B}_2 decreases these errors 100-fold, down to 3×10^{-6} . For multipolar radiation with $\ell = 4$, a factor of about 3600 in accuracy is gained as one goes from \mathcal{B}_1

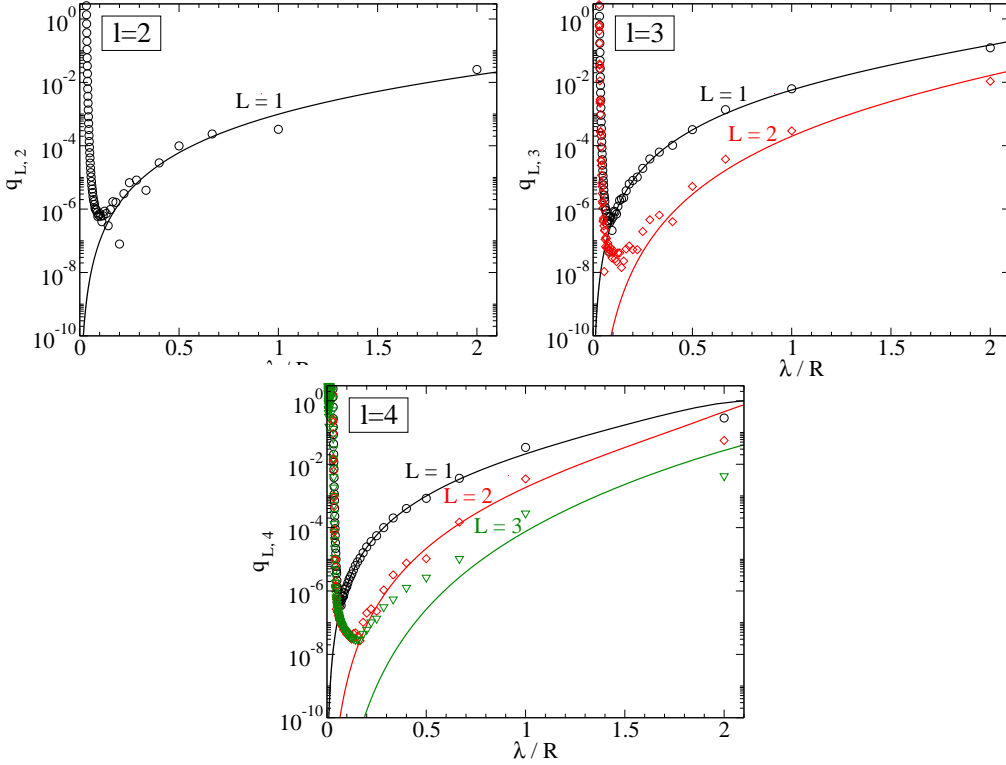


Figure 9. Reflection coefficients as a function of λ/R (where R is the outer boundary radius and λ is the wavelength) for odd-parity linearized solutions to the Einstein equations, with absorbing BCs \mathcal{B}_L of selected orders L . Curves denote coefficients $q_{L,\ell}$ calculated from equation 96 of [1], and points denote coefficients computed from numerical evolutions of linearized-wave initial data. Different panels correspond to solutions with different values of the angular momentum number ℓ . Note that $\mathcal{B}_{L=\ell}$ is perfectly absorbing and hence $q_{L,\ell} = 0$.

(where the error is 9×10^{-4}) to \mathcal{B}_3 (where the error is 2.5×10^{-7}).

Figure 9 also shows that the predicted and numerical reflection coefficients agree well except for small values of λ/R and small values of the reflection coefficient. The discrepancies are likely to be caused by a combination of different effects. (i) We have computed the numerical reflection coefficients from a fully nonlinear evolution whereas the predictions are only valid in linearized theory. These nonlinear effects should become less important as the amplitude of the wave is decreased. (ii) Numerical roundoff error becomes important for small values of the difference between the exact and numerical solution (visible in figures 5, 6 and 8). (iii) There is an accumulated error of spurious reflections passing through the origin and reflecting again, which is not accounted for in the theoretical reflection coefficients. One can see this in the secondary pulse at $t \approx 45$ in figures 5, 6 and 8. (iv) For $\lambda\ell/(2\pi R) \gtrsim 1$, the theoretical predictions for the reflection coefficients start to break down because the ingoing solutions used for the calculation in [1] are not valid as the wave approaches $r = 0$.

4. Conclusions

An algorithm for numerically implementing the higher-order absorbing BCs \mathcal{B}_L for Einstein's equations presented in [1] has been defined, tested, and shown to work. Our method is based on a reformulation of the BCs in terms of the gauge-invariant RWZ scalars. This approach relies on the assumption that close to the outer boundary, the Einstein equations can be linearized about a given background spacetime, which in this paper is taken to be flat. It also requires a spherical outer boundary. A key feature of our algorithm is the introduction of auxiliary variables intrinsic to the boundary, a technique familiar from the fields of, for example, computational electromagnetism and acoustics.

We have used a generalized harmonic formulation of the Einstein equations [19]; however, it should be straightforward to adapt our algorithm to different formulations, with minor modifications. Similarly, our use of spectral numerical methods is not an essential ingredient. Our boundary algorithm can be added to any existing numerical relativity code in a modular way: all that needs to be done is to implement the auxiliary evolution system at the boundary and provide for the necessary exchange of information with the main evolution system. In order to estimate the additional computational cost in doing so, we note that the number of auxiliary variables $w_{k,\ell m}^{(\pm)}$ that need to be evolved for the absorbing BC \mathcal{B}_L (which is perfectly absorbing for all multipoles $\ell \leq L$) is $2L(L+1)^2$. (The ranges are $1 \leq k \leq L$, $0 \leq \ell \leq L$, $-\ell \leq m \leq \ell$.) E.g. for $L = 3$, this amounts to 96 functions (of time only), which is small compared to a typical number of grid points in the interior domain.

We have implemented our method in the Caltech-Cornell SpEC code and have tested it by evolving initial data with not only quadrupolar ($\ell = 2$), but also higher multipolar ($\ell = 3, 4$) radiation, imposing the hierarchy of BCs \mathcal{B}_L with $L \leq \ell$. We use linearized solutions of the Einstein equations [21, 22] as initial data, and evolve these in a fully nonlinear code. We demonstrate that with decreasing amplitude of the radiation in the initial data, and perfectly absorbing BCs $\mathcal{B}_{L=\ell}$, the numerical solution decays at least quadratically to the exact linearized solution, as expected. For $\mathcal{B}_{L<\ell}$, the difference between the numerical and exact solutions decays only linearly as the amplitude is decreased, indicating that linear, spurious reflections are being introduced into the solution. We have estimated the magnitude of these spurious reflections in our numerical simulations and find good agreement with the theoretical reflection coefficients derived in [1], within the range of validity of the two calculations. For multipolar radiation with $\ell = 3$ or 4, we have seen that even without imposing a perfectly absorbing BC $\mathcal{B}_{L=\ell}$, one can decrease the reflections off the outer boundary dramatically by increasing the order L of the BC \mathcal{B}_L . For instance, for an outer boundary radius of twice the wavelength, $R = 2\lambda$, and $\ell = 3$, we achieve a 100-fold decrease in reflection by using \mathcal{B}_2 rather than \mathcal{B}_1 .

The most important application of our work is to the simulation of isolated systems, such as coalescing binary black holes. In these simulations, the most sophisticated BC on the gravitational radiation currently in use is the freezing- Ψ_0 BC [23, 24, 25, 26, 27, 28, 29], which corresponds to \mathcal{B}_1 . Note that the ratio of the wavelength to the outer boundary radius in the numerical tests presented in this article is $\lambda/R \sim 0.1$; such a small value for λ/R makes it easy to ensure that the BCs are consistent with the initial data because the radiation vanishes at the outer boundary. In contrast, for binary black hole simulations, λ/R is much closer to unity, in particular during the inspiral phase. One can see from the graphs in figure

9 that errors due to reflections with imperfectly absorbing BCs (including \mathcal{B}_1) are several orders of magnitude larger at, say, $\lambda/R = 0.5$ than they are at $\lambda/R = 0.1$. Furthermore, the majority of current binary black hole simulations use far cruder BCs on the gravitational radiation than \mathcal{B}_1 : Typically, a sequence of adaptive mesh refinement [37] grids of decreasing resolution are used that extend out to larger and larger radii (see e.g. [38, 39, 40, 41, 42]). On the coarsest grid, the waves are no longer properly resolved, and some *ad hoc* BC (such as a Sommerfeld BC) is imposed. It is clear that this approach will cause spurious reflections, and given the results of [27], we suspect that these will be considerably larger than those caused by \mathcal{B}_1 .

Inspiralling and merging equal mass non-spinning binary black holes emit predominantly quadrupolar ($\ell = 2$) radiation. For a typical outer boundary location used in numerical simulations of these events, $R = 2\lambda$, the errors due to spurious reflections of quadrupolar radiation with \mathcal{B}_1 are predicted in [1] to be 6×10^{-5} , which seems very small. However, these reflections may interact with the evolution in such a way as to result in an accumulating phase error. For instance, the runs in [28] showed phase errors of a few hundredths of a radian which were attributed to the outer boundary location. Moreover, as the mass ratio M_1/M_2 deviates from unity, the energy emitted in non-quadrupolar modes rapidly increases: while for $M_1/M_2 = 1$, less than 0.1 per cent of the energy is emitted with $\ell > 2$, this fraction increases to a few per cent for $M_1/M_2 = 2$ and exceeds 10 per cent for the still fairly modest mass ratio $M_1/M_2 = 4$ [43, 44]. Because \mathcal{B}_1 has larger reflection coefficients at a given value of λ/R for $\ell > 2$ modes than for $\ell = 2$ modes (cf. figure 9), this BC will not perform as well for unequal mass binary black hole simulations; in these cases, the higher-order BCs presented in this paper will be even more important than they are for equal mass simulations. Finally, when considering the merit of the higher-order BCs on simulations containing different modes (ℓ, m) , one needs to remember that the wavelength of a mode depends on the value of m . During the inspiral, modes with smaller $|m|$ have larger wavelengths λ (typically in proportion to $1/|m|$), and therefore the ratio of wavelength to boundary radius, λ/R , depends on m . From figure 9 we then deduce that modes with the same ℓ but different m will have different reflection coefficients. For example, the $(2, 1)$ mode has been shown to contribute significantly to the unequal mass binary black hole inspiral radiation [43]. Because its wavelength is longer than for the $(2, 2)$ mode, the reflection coefficient for \mathcal{B}_1 will be correspondingly higher.

For these reasons, we are confident that higher-order BCs will improve the accuracy of long-term unequal mass binary black hole simulations. Whether such an improvement is desirable will of course depend on the precision requirements for the computed waveforms. Parameter estimation for LIGO requires phase errors of hundredths of a radian [45], and LISA will require yet more accurate waveforms.

Our work can also be applied to the problem of Cauchy-perturbative matching. In this approach, one matches solutions to the full nonlinear Einstein equations on an interior spatial domain to solutions of the linearized equations on an exterior domain extending out to large radii. These linearized equations can be represented for instance by the gauge-invariant RWZ equations. The question now arises as to how one should impose outer BCs on the Einstein equations in the interior with boundary data computed from the exterior linearized solution. Sections 2.4 and 2.5 contain a specific prescription for how this can be done.

In future work, we plan to generalize our algorithm by (i) including first-order corrections in M/R for the curvature and backscatter on a Schwarzschild background

spacetime (of mass M), (ii) allowing for arbitrary coordinates of the background spacetime, and (iii) adapting the algorithm to more general (i.e., not necessarily spherical) boundary shapes. The generalized RWZ formalism [18] upon which our calculations are based and the absorbing BCs formulated in [1, 2] allow for such generalizations. In more realistic situations where an exact solution is not at hand, one can assess the quality of the BCs by comparing with a numerically computed (fully nonlinear) reference solution on a large domain [27]. Ultimately, we plan to apply our implementation of absorbing BCs to binary black hole simulations using the Caltech-Cornell SpEC code.

Acknowledgments

We thank James Bardeen, Edvin Deadman, Lee Lindblom, Richard Matzner, Olivier Sarbach, Erik Schnetter, John Stewart and Manuel Tiglio for insightful suggestions and discussions during the course of this work, and Keith Matthews for use of and help with his ODE integration code. The numerical simulations presented here were performed using the Spectral Einstein Code (SpEC) developed at Caltech and Cornell primarily by Larry Kidder, Harald Pfeiffer and Mark Scheel.

This work was supported in part by grants to Caltech from the Sherman Fairchild Foundation and the Brinson Foundation, by NSF grants DMS-0553302, PHY-0601459, PHY-0652995, and by NASA grant NNG05GG52G. LTB was also supported by grants NSF PHY 03 54842 and NASA NNG 04GL37G to the University of Texas at Austin. OR gratefully acknowledges funding through a Research Fellowship at King's College Cambridge.

Appendix A. Conversion to spin-weighted harmonics

The spin-weighted spherical harmonics [46] ${}_s Y_{\ell m}(\theta, \phi)$ can be constructed from the standard spherical harmonics $Y_{\ell m}$ recursively using the relations

$${}_0 Y_{\ell m} = Y_{\ell m}, \quad (\text{A.1})$$

$${}_{s+1} Y_{\ell m} = [(\ell - s)(\ell + s + 1)]^{-1/2} \bar{\partial}_s Y_{\ell m}, \quad (\text{A.2})$$

$${}_{s-1} Y_{\ell m} = -[(\ell + s)(\ell - s + 1)]^{-1/2} \bar{\partial}_s Y_{\ell m}. \quad (\text{A.3})$$

The operators $\bar{\partial}$ and $\bar{\bar{\partial}}$ are defined by

$$\bar{\partial}_s Y_{\ell m} \equiv (-\partial_\theta - i \csc \theta \partial_\phi + s \cot \theta) {}_s Y_{\ell m}, \quad (\text{A.4})$$

$$\bar{\bar{\partial}}_s Y_{\ell m} \equiv (-\partial_\theta + i \csc \theta \partial_\phi - s \cot \theta) {}_s Y_{\ell m}. \quad (\text{A.5})$$

Next we set up a tetrad $\mathbf{e}_\mu = (\mathbf{t}, \mathbf{r}, \mathbf{m}, \bar{\mathbf{m}})$. (Greek indices μ, ν, \dots from the middle of the alphabet denote tetrad indices.) In components with respect to spherical polar coordinates (t, r, θ, ϕ) ,

$$t_\alpha = (1, 0, 0, 0), \quad r_\alpha = (0, 1, 0, 0), \quad m_\alpha = \frac{r}{\sqrt{2}}(0, 0, 1, i \sin \theta), \quad (\text{A.6})$$

and $\bar{\mathbf{m}}$ is the complex conjugate of \mathbf{m} . An arbitrary rank-2 tensor \mathbf{T} can be expanded as

$$\mathbf{T} = \sum_{\ell, m, \mu, \nu} T_{\ell m}^{\mathbf{e}_\mu \mathbf{e}_\nu} {}_s(\mathbf{e}_\mu, \mathbf{e}_\nu) Y_{\ell m} \mathbf{e}_\mu \otimes \mathbf{e}_\nu. \quad (\text{A.7})$$

Here the spin weight is defined by $s(\mathbf{e}_\mu, \mathbf{e}_\nu) = s(\mathbf{e}_\mu) + s(\mathbf{e}_\nu)$ where $s(\mathbf{m}) = -1$, $s(\bar{\mathbf{m}}) = +1$, and $s(\mathbf{t}) = s(\mathbf{r}) = 0$. The SpEC code provides routines that compute the expansion coefficients $T_{\ell m}^{\mathbf{e}_\mu \mathbf{e}_\nu}$ in (A.7) for a given tensor \mathbf{T} .

The basis harmonics defined in (12) can be written as

$$Y_{A,\ell m} = -\frac{\sqrt{\ell(\ell+1)}}{\sqrt{2}r}({}_1Y_{\ell m}\bar{m}_A - {}_{-1}Y_{\ell m}m_A), \quad (\text{A.8})$$

$$S_{A,\ell m} = -\frac{i\sqrt{\ell(\ell+1)}}{\sqrt{2}r}({}_1Y_{\ell m}\bar{m}_A + {}_{-1}Y_{\ell m}m_A), \quad (\text{A.9})$$

$$Y_{AB,\ell m} = \frac{\sqrt{\lambda\ell(\ell+1)}}{2r^2}({}_2Y_{\ell m}\bar{m}_A\bar{m}_B + {}_{-2}Y_{\ell m}m_Am_B), \quad (\text{A.10})$$

$$S_{AB,\ell m} = \frac{i\sqrt{\lambda\ell(\ell+1)}}{2r^2}({}_2Y_{\ell m}\bar{m}_A\bar{m}_B - {}_{-2}Y_{\ell m}m_Am_B). \quad (\text{A.11})$$

(Recall that $\lambda = (\ell-1)(\ell+2)$.) We also have $\hat{g}_{AB} = 2r^{-2}m_{(A}\bar{m}_{B)}$. Using these relations it is straightforward to express the amplitudes of the perturbation (13)–(14) and (19)–(21) in terms of the expansion coefficients $\delta g_{\ell m}^{\mathbf{e}_\mu \mathbf{e}_\nu}$,

$$h_{t,\ell m} = \frac{ir}{\sqrt{2\ell(\ell+1)}}(\delta g_{\ell m}^{\mathbf{t}\bar{\mathbf{m}}} + \delta g_{\ell m}^{\mathbf{t}\mathbf{m}}), \quad (\text{A.12})$$

$$h_{r,\ell m} = \frac{ir}{\sqrt{2\ell(\ell+1)}}(\delta g_{\ell m}^{\mathbf{r}\bar{\mathbf{m}}} + \delta g_{\ell m}^{\mathbf{r}\mathbf{m}}), \quad (\text{A.13})$$

$$k_{\ell m} = \frac{-ir^2}{2\sqrt{\lambda\ell(\ell+1)}}(\delta g_{\ell m}^{\bar{\mathbf{m}}\bar{\mathbf{m}}} - \delta g_{\ell m}^{\mathbf{m}\mathbf{m}}), \quad (\text{A.14})$$

$$H_{tt,\ell m} = \delta g_{\ell m}^{\mathbf{t}\mathbf{t}}, \quad (\text{A.15})$$

$$H_{tr,\ell m} = \delta g_{\ell m}^{\mathbf{t}\mathbf{r}}, \quad (\text{A.16})$$

$$H_{rr,\ell m} = \delta g_{\ell m}^{\mathbf{r}\mathbf{r}}, \quad (\text{A.17})$$

$$Q_{t,\ell m} = \frac{-r}{\sqrt{2\ell(\ell+1)}}(\delta g_{\ell m}^{\mathbf{t}\bar{\mathbf{m}}} - \delta g_{\ell m}^{\mathbf{t}\mathbf{m}}), \quad (\text{A.18})$$

$$Q_{r,\ell m} = \frac{-r}{\sqrt{2\ell(\ell+1)}}(\delta g_{\ell m}^{\mathbf{r}\bar{\mathbf{m}}} - \delta g_{\ell m}^{\mathbf{r}\mathbf{m}}), \quad (\text{A.19})$$

$$K_{\ell m} = \delta g_{\ell m}^{\bar{\mathbf{m}}\bar{\mathbf{m}}}, \quad (\text{A.20})$$

$$G_{\ell m} = \frac{1}{\sqrt{\lambda\ell(\ell+1)}}(\delta g_{\ell m}^{\bar{\mathbf{m}}\bar{\mathbf{m}}} + \delta g_{\ell m}^{\mathbf{m}\mathbf{m}}). \quad (\text{A.21})$$

References

- [1] Buchman L T and Sarbach O C A 2006 Towards absorbing outer boundaries in general relativity *Class. Quantum Grav.* **23** 6709–6744
- [2] Buchman L T and Sarbach O C A 2007 Improved outer boundary conditions for Einstein's field equations *Class. Quantum Grav.* **24** S307–S326
- [3] Bayliss A and Turkel E 1980 Radiation boundary conditions for wave-like equations *Comm. Pure Appl. Math.* **33** 707–725
- [4] Novak J and Bonazzola S 2004 Absorbing boundary conditions for simulation of gravitational waves with spectral methods in spherical coordinates *J. Comput. Phys.* **197** 86–196
- [5] Alpert B, L G and Hagstrom T 2000 Rapid evaluation of nonreflecting boundary kernels for time-domain wave propagation *SIAM J. Numer. Anal.* **37** 1138–1164
- [6] Lau S L 2004 Rapid evaluation of radiation boundary kernels for time-domain wave propagation on black holes: theory and numerical methods *J. Comput. Phys.* **199** 376–422

- [7] Lau S L 2004 Rapid evaluation of radiation boundary kernels for time-domain wave propagation on black holes: implementation and numerical tests *Class. Quantum Grav.* **21** 4147–4192
- [8] Lau S L 2004 Analytic structure of radiation boundary kernels for black hole perturbations *J. Math. Phys.* **46** 102503
- [9] Abrahams A M *et al.* (Binary Black Hole Grand Challenge Alliance) 1998 Gravitational wave extraction and outer boundary conditions by perturbative matching *Phys. Rev. Lett.* **80** 1812–1815
- [10] Rupright M E, Abrahams A M and Rezzolla L 1998 Cauchy-perturbative matching and outer boundary conditions I: Methods and tests *Phys. Rev. D* **58** 044005
- [11] Rezzolla L, Abrahams A M, Matzner R A, Rupright M E and Shapiro S L 1999 Cauchy-perturbative matching and outer boundary conditions: Computational studies *Phys. Rev. D* **59** 064001
- [12] Zink B, Pazos E, Diener P and Tiglio M 2006 Cauchy-perturbative matching reexamined: Tests in spherical symmetry *Phys. Rev. D* **73** 084011
- [13] Winicour J 2005 Characteristic evolution and matching *Living Rev. Rel.* **8**(10)
- [14] Frauendiener J 2004 Conformal infinity *Living Rev. Rel.* **7**(1)
- [15] Hagstrom T and Hariharan S 1998 A formulation of asymptotic and exact boundary conditions using local operators *Appl. Numer. Math.* **27** 403–416
- [16] Huan R and Thompson L 2000 Accurate radiation boundary conditions for the time-dependent wave equation on unbounded domains *Int. J. Numer. Meth. Engng.* **47** 1569–1603
- [17] Givoli D 2001 High-order nonreflecting boundary conditions without high-order derivatives *J. Comput. Phys.* **170** 849–870
- [18] Sarbach O and Tiglio M 2001 Gauge-invariant perturbations of Schwarzschild black holes in horizon-penetrating coordinates *Phys. Rev. D* **64** 084016
- [19] Lindblom L, Scheel M A, Kidder L E, Owen R and Rinne O 2006 A new generalized harmonic evolution system *Class. Quantum Grav.* **23** S447–S462
- [20] Kreiss H O and Winicour J 2006 Problems which are well posed in a generalized sense with applications to the Einstein equations *Class. Quantum Grav.* **16** S405–S420
- [21] Teukolsky S A 1982 Linearized quadrupole waves in general relativity and the motion of test particles *Phys. Rev. D* **26** 745–750
- [22] Rinne O 2009 Explicit solution of the linearized Einstein equations in the transverse-traceless gauge for all multipoles *Class. Quantum Grav.* **26** 048003
- [23] Bardeen J M and Buchman L T 2002 Numerical tests of evolution systems, gauge conditions, and boundary conditions for 1D colliding gravitational plane waves *Phys. Rev. D* **65** 064037
- [24] Kidder L E, Lindblom L, Scheel M A, Buchman L T and Pfeiffer H P 2005 Boundary conditions for the Einstein evolution system *Phys. Rev. D* **71** 064020
- [25] Sarbach O and Tiglio M 2005 Boundary conditions for Einstein’s field equations: Analytical and numerical analysis *J. Hyp. Differ. Eqn.* **2** 839–883
- [26] Scheel M A, Pfeiffer H P, Lindblom L, Kidder L E, Rinne O and Teukolsky S A 2006 Solving Einstein’s equations with dual coordinate frames *Phys. Rev. D* **74** 104006
- [27] Rinne O, Lindblom L and Scheel M A 2007 Testing outer boundary treatments for the Einstein equations *Class. Quantum Grav.* **24** 4053–4078
- [28] Boyle M, Brown D A, Kidder L E, Mroué A H, Pfeiffer H P, Scheel M A, Cook G B and Teukolsky S A 2007 High-accuracy comparison of numerical relativity simulations with post-Newtonian expansions *Phys. Rev. D* **76** 124038
- [29] Scheel M A, Boyle M, Chu T, Kidder L E, Matthews K D and Pfeiffer H P 2009 High-accuracy waveforms for binary black-hole inspiral, merger, and ringdown *Phys. Rev. D* **79** 024003
- [30] Darboux J G 1915 *Leçons sur la théorie générale des surfaces et les applications géométriques du calcul infinitésimal* vol 2 (Paris: Gauthier-Villars) livre 4, chapitre 3: L’équation d’Euler et de Poisson
- [31] Kreiss H O, Reula O, Sarbach O and Winicour J 2007 Well-posed initial-boundary value problem for the harmonic Einstein equations using energy estimates *Class. Quantum Grav.* **24** 5973–5984
- [32] Ruiz M, Rinne O and Sarbach O 2007 Outer boundary conditions for Einstein’s field equations in harmonic coordinates *Class. Quantum Grav.* **24** 6349
- [33] Matsushima T and Marcus P S A spectral method for polar coordinates *J. Comput. Phys.* **120** 365–374
- [34] Hesthaven J S 2000 Spectral penalty methods *Appl. Num. Math.* **33** 23–41
- [35] Rinne O 2006 Stable radiation-controlling boundary conditions for the generalized harmonic Einstein equations *Class. Quantum Grav.* **23** 6275–6300
- [36] Rinne O and Sarbach O 2007 Private communication

- [37] Berger M J and Olinger J 1984 Adaptive mesh refinement for hyperbolic partial differential equations *J. Comput. Phys.* **53** 484–512
- [38] Baker J G, Centrella J, Choi D I, Koppitz M and van Meter J 2006 Gravitational-wave extraction from an inspiraling configuration of merging black holes *Phys. Rev. Lett.* **96**(11) 111102
- [39] Diener P, Herrmann F, Pollney D, Schnetter E, Seidel E, Takahashi R, Thornburg J and Ventrella J 2006 Accurate evolution of orbiting binary black holes *Phys. Rev. Lett.* **96** 121101
- [40] Husa S, González J A, Hannam M, Brüggmann B and Sperhake U 2008 Reducing phase error in long numerical binary black hole evolutions with sixth order finite differencing *Class. Quantum Grav.* **25** 105006
- [41] Lousto C O and Zlochower Y 2008 Foundations of multiple black hole evolutions *Phys. Rev. D* **77** 024034
- [42] Hinder I, Herrmann F, Laguna P and Shoemaker D 2008 Comparisons of eccentric binary black hole simulations with post-Newtonian models (*E-print* <http://www.arxiv.org/abs/0806.1037>)
- [43] Berti E, Cardoso V, Gonzalez J A, Sperhake U, Hannam M, Husa S and Brüggmann B 2007 Inspiral, merger, and ringdown of unequal mass black hole binaries: A multipolar analysis *Phys. Rev. D* **76** 064034
- [44] Berti E, Cardoso V, Gonzalez J A, Sperhake U and Brüggmann B 2008 Multipolar analysis of spinning binaries *Class. Quantum Grav.* **25** 114035
- [45] Lindblom L, Owen B J and Brown D A 2008 Model Waveform Accuracy Standards for Gravitational Wave Data Analysis *Phys. Rev.* **D78** 124020
- [46] Newman E T and Penrose R 1966 Note on the Bondi–Metzner–Sachs group *J. Math. Phys.* **7** 863–870